Real-time Simulation of Electric Vehicle Powertrain: Hardware-in-the-Loop (HIL) Testbed for Cyber-Physical Security

Bowen Yang
College of Engineering
University of Georgia
Athens, Georgia USA 30602
Email: bowen.yang@uga.edu

Lulu Guo
College of Engineering
University of Georgia
Athens, Georgia USA 30602
Email: lulu.guo@uga.edu

Jin Ye
College of Engineering
University of Georgia
Athens, Georgia USA 30602
Email: jin.ye@uga.edu

***Abstract*—With the fast development of vehicular on-board communication networks, modern electric vehicles are exposed to potential threats from cyber networks. To secure the vehicle safety and efficiency, advanced simulation platforms for cyber-physical security research are of urgent desires. In this paper, we propose a hardware-in-the-loop real-time simulation testbed for electric vehicle powertrain cyber-physical security research. The testbed includes multiple physical domains of an electric vehicle powertrain: electric drive systems, mechanical transmission system, and vehicle control units. An advanced energy consumption monitor that calculates the system energy and power information is constructed. Besides, other critical details like tire-road interactions and road and aerodynamic friction information are also taken into considerations. Furthermore, the testbed is highly modularized, which makes it simple to realize hardware-in-the-loop simulation. All of these features make it an accurate, simple, and effective testbed for electric vehicle powertrain research on system performance, efficiency, reliability, and cyber-physical security.**

I. Introduction

Last decade has witnessed the fast progress of both electrification and intellectualization of modern vehicles. Nevertheless, the accompanying concerns about immature on-board electrical and intelligent technologies remains a large obstacle for modern techniques to completely replacing the traditional vehicular technologies. Recently, an increasing amount of work has been devoted to cyber-physical security research for modern electric vehicles. In 2010, Koscher et al. experimentally evaluate the cyber-physical security issues on a modern automobile and demonstrate the fragility of the underlying system structure. [1]. In addition, the impact of cyber attacks on electric drives are studied in [2] and [3]; and in [4]–[11], both model-based and data-driven approaches for cyber-physical security are studied as well. Furthermore, due to the complexity of the system configuration and the high cost of manufacturing real-world testbed, real-time and hardware-in-the-loop (HIL) simulation have been widely adopted in the research and development for advanced on-board systems such as electrified powertrain and on-board communication networks. For example, [12] proposed a simple HIL simulation system for the induction motor-based powertrain coupled to a DC machine-based load torque emulator taking into account the electric vehicle mechanics and aerodynamics; [13] adopted HIL simulation for developing advanced control strategy for a pure electric vehicle; [14] constructed the battery model and corresponding battery management system (BMS) in the real-time simulation environment; [15] used HIL to test an electric propulsion system used in a mild hybrid electric vehicle powertrain.

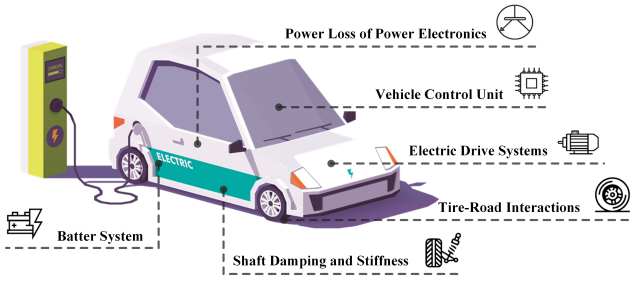

Fig. 1: General diagram of an electric vehicle.

Due to the fact that most of the relevant research about electric vehicle powertrain still focuses on developing advanced and optimal control strategies, most of the simulation platforms only discuss one subsystem in detail, such as battery management systems (BMSs) or electric drive systems (EDSs). For the purpose of reducing computation burden, many nonlinear features have been neglected in designing specific systems. When considering the problems of cyber-physical security, more comprehensive simulation platform is needed in the following aspects:

1) Cyber-physical attacks are considered as random behaviors that could occur anywhere in the powertrain;
2) The impact of cyber-physical attacks will not be limited to one specific system, but the entire powertrain;
3) System nonlinearity is one of the features the cyber-physical attackers could exploit to cause more drastic damage;
4) Cyber-physical attacks could have both short and long term impacts on the system.

978-1-7281-4629-4/20/$31.00 ©2020 IEEE

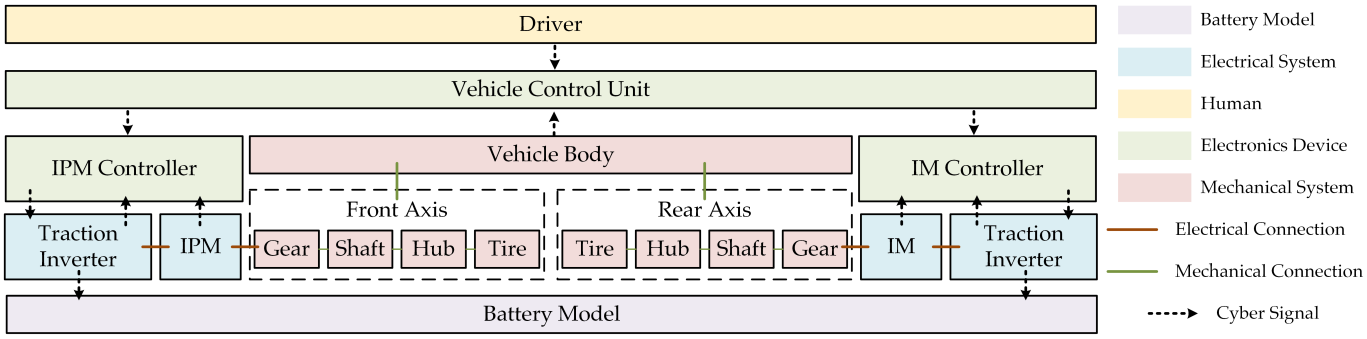

Fig. 2: System diagram of dual-motor based electric vehicle powertrain

Therefore, to accurately reflect the impact of different cyber-physical attacks and evaluate the system reliability and security, an advanced simulation model with the ability of real-time simulation and details like tire-road interactions, high-frequency switching of power electronics and electrical-thermal coupling within the electric drive systems is required.

In this paper, we use OPAL-RT and MATLAB Simulink to develop a nonlinear real-time simulation model of a dual-motor based electric vehicle powertrain, which includes all the details shown in Fig. 1. More specifically, it includes multiple physical domains of an electric vehicle powertrain: electric drive systems, mechanical transmission system, battery system, and vehicle control units. Meanwhile, an advanced energy consumption monitor that calculates the system energy and power information is constructed. In addition, other critical details like tire-road interactions and road and aerodynamic friction information are also taken into considerations. The remaining article will be organized as follow: section II will introduce the general system structure; section III will describe the interior permanent magnet synchronous machine (IPM) based EDS; vehicle plant model will be described in section IV; energy monitor will be described in section V; and section VI, VII will list the simulation results and summarize the conclusions.

II. Dual-Motor Based Electric Vehicle Powertrain

In this platform, we adopted a widely used powertrain structure, the dual-motor based powertrain. The system diagram is shown in Fig. 2, which includes two different motors driving the front and real axis, respectively. As shown in Fig. 2, the front wheel is driven by an interior permanent magnet synchronous machine (IPM), and the rear wheel is driven by an induction machine (IM). Each electric machine has its own controller and traction inverter to control the power flows between machines and the battery. In addition, the vehicle control unit (VCU) gathers information from the driver's demands and the vehicle body, such as the vehicle speed, and then provides the torque reference to each of the motor controllers. The detailed models of each subsystem will be described in the following sections.

III. IPM Based EDS Model

Due to the high power density and smooth torque production, IPM has been widely used as the traction motor of electric vehicles. Fig. 4 shows the configuration of the IPM based EDS. Referring to the torque command received from the vehicle control unit (VCU) and the feedback signals gathered from sensors, a current controller is adopted alongside the maximum torque per ampere (MTPA) algorithm to generate the pulse width modulation (PWM) signals, which control the traction inverter fed by a DC power supply and then drive the IPM. In this paper, for the purpose of achieving real-time simulation, the eFPGA solver and eHS solver of OPAL-RT is adopted to solve the machine and power electronics models and to realize the simulation with a time step of $0.5\mu s$; and the controller model is constructed by MATLAB Simulink, which is run in the CPU with a time step of $25\mu s$.

The simulation configuration is shown in Fig. 3. The reason why adopting eFPGA and eHS solver is that the ability of parallel computing of FPGA enables simulation with time step as low as $0.25\mu s$, which makes it possible for power electronics models with 10kHz to 200kHz switching frequency to run in real-time. As shown in Fig. 3, the electric circuits of traction inverter is solved in eHS, and the IPM is modeled by its Variable D-Q model (VDQ) from eFPGA library, which is derived by the following equations under direct-quadrature-zero

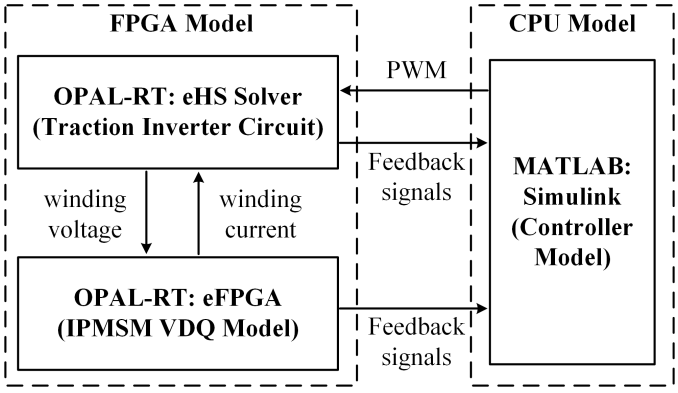

Fig. 3: The configuration of the EDS model

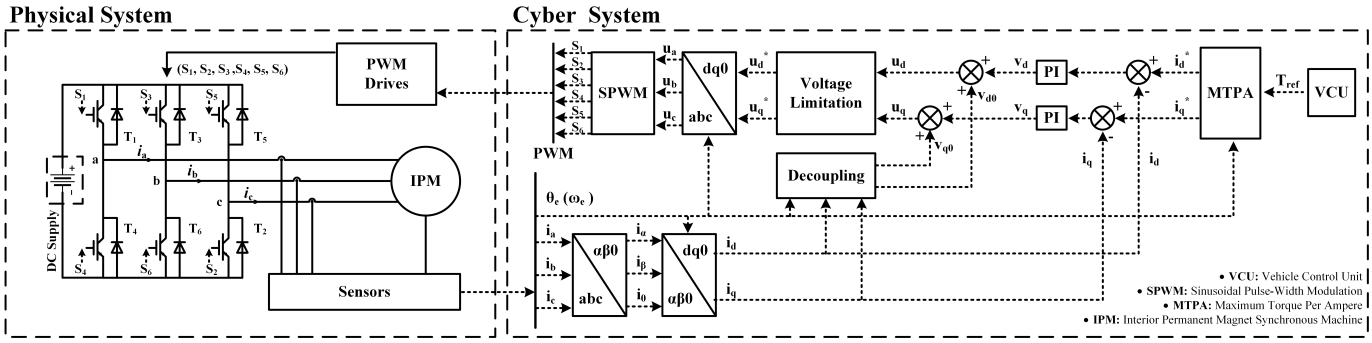

Fig. 4: Schematic diagram of the IPM drive including both cyber system (control algorithms) and physical system (hardware).

(DQZ) reference frame:

$$u_d = R_s i_d + L_d(i_d, i_q)\frac{di_d}{dt} - \omega_e L_q(i_d, i_q) i_q \tag{1}$$

$$u_q = R_s i_q + L_q(i_d, i_q)\frac{di_q}{dt} + \omega_e (L_d(i_d, i_q) i_d + \phi_{pm}) \tag{2}$$

$$T_e = \frac{3}{2} p(\phi_{pm} i_q + (L_d(i_d, i_q) - L_q(i_d, i_q)) i_d i_q) \tag{3}$$

where $u_d,\ u_q,\ i_d,\ i_q,\ \phi_{pm}$ are the d-axis and q-axis voltage and current vectors, and flux linkage generated by permanent magnet, respectively; p is the number of pole pairs; and $L_d(i_d, i_q),\ L_q(i_d, i_q)$ are the nonlinear inductance of d- and q- axis acquired by 2-D look-up tables.

Meanwhile, the MTPA algorithm is derived from the following optimization problem:

$$\min \quad i_d^2 + i_q^2 \tag{4}$$

$$s.t. \quad \begin{cases} \frac{3}{2} p(\phi_{pm} i_q + (L_d(i_d, i_q) - L_q(i_d, i_q)) i_d i_q) = Te \\ \sqrt{i_d^2 + i_q^2} \le I_{am} \\ \sqrt{u_d^2 + u_q^2} \le U_{am} \end{cases} \tag{5}$$

where T_e is the anticipating torque and $u_d,\ u_q$ are obtained by Eq. (1) and Eq. (2).

IV. Vehicle Plant Model

To reflect the mechanical characteristics as detailed as possible, the vehicle plant model covers shaft stiffness, load distributions between the front and rear axis, the tire-road interactions, rolling resistance, gradient resistance, and aerodynamic resistance. The shaft model is modeled as:

$$T = K_s \cdot \phi \qquad \text{(rotational spring)} \tag{6}$$

$$T = K_d \cdot \Omega \qquad \text{(rotational damper)} \tag{7}$$

where T is the torque applied to the shaft, K_s, K_d are the damping coefficients, and ϕ, Ω are the rotational angle and speed, respectively. The tire-road interaction is derived from the tire magic formula. First of all, the dimensions of vehicle plant and the force conditions of the tire is shown in Fig. 5; and the traction force, the tire slip κ and nominal load distribution $F_{z-front}, F_{z-rear}$ are defined:

$$\kappa = \frac{|r_w \cdot \Omega - v_x|}{|v_x|} \tag{8}$$

$$F_{z-front} = F_z \cdot (1 - \frac{l_f}{l}) - \frac{h}{l} \cdot F_t \tag{9}$$

$$F_{z-rear} = F_z \cdot \frac{l_f}{l} + \frac{h}{l} \cdot F_t \tag{10}$$

where F_z is the total nominal load, and F_t is the vehicle total traction force. Then, according to the magic formula of tire-road interactions, the horizontal traction force F_x is defined:

$$F_x = F_{z-j} \cdot D \cdot \sin(C \cdot \arctan(B\kappa - E \cdot (B\kappa - \arctan(B\kappa)))) \tag{11}$$

where B, C, D, E are the constant coefficients of magic formula, which is dependent on the load conditions, and F_{z-j} is the nominal load distribution defined in Eq. (9), Eq. (10), (j denotes the front or the rear wheel).

In addition, the rolling resistance, gradient resistance and the aerodynamic resistance are also considered as the road resistance force in this model, which are derived from:

$$F_g = k_f \cdot \cos\alpha \qquad \text{(rolling resistance)} \tag{12}$$

$$F_r = m \cdot g \cdot \sin\alpha \qquad \text{(gradient resistance)} \tag{13}$$

$$F_w = \frac{1}{2} C_d \cdot A \cdot \rho \cdot v^2 \qquad \text{(aerodynamic resistance)} \tag{14}$$

where k_f is the rolling resist coefficient, m is the mass of the vehicle, g is the acceleration of gravity; α is the road gradient, and C_d, A, ρ, v are the drag coefficient, reference area, air density and vehicle speed, respectively.

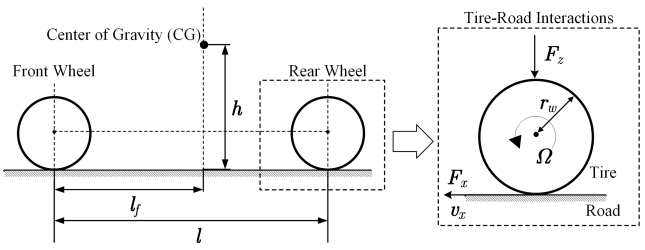

Fig. 5: Vehicle dimensions and the force conditions

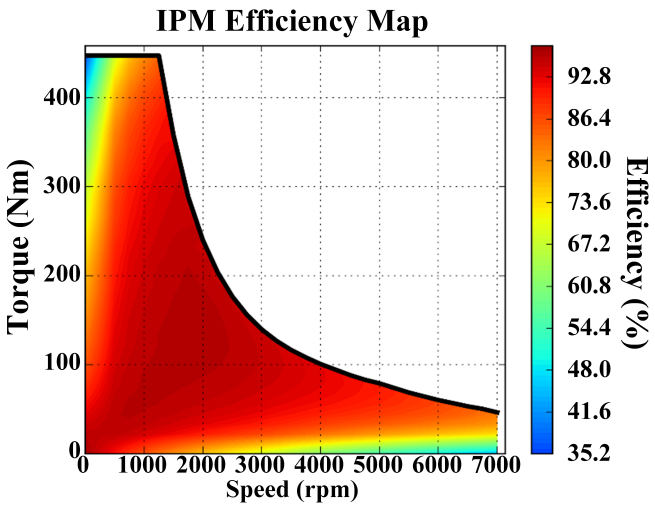

Fig. 6: Efficiency map of IPM generated by Finite Element Analysis.

V. Energy Consumption Monitor

In the application of automobiles, energy efficiency is always a crucial topic. Therefore, in this platform, we construct an energy consumption monitor to calculate the instant energy information for further analysis. The monitor is divided into four parts: motor loss, inverter loss, mechanical loss, and battery loss. Each part will be elaborated more as follows:

A. Motor Loss

The power loss in electric machines includes winding copper loss, iron core loss, solid loss, and mechanical loss. Due to the nonlinearity of electric machines and the difficulties of power calculations, we use ANSYS to generate the efficiency map of the electric machines by conducting Finite Element Analysis. Fig. 6 shows the resulted IPM efficiency map.

B. Traction Inverter Loss

Recently, with the pervasive adoption of power electronics devices in automobile applications, the energy efficiency of the traction inverters is getting increasing attention. In this platform, we use the electro-thermal model in [16], [17] to calculate the instant power loss of the traction motor. The detailed calculation procedures are shown in Fig. 7.

C. Mechanical Loss

Due to the fact that the tire-road interactions are taking into consideration, the mechanical loss becomes another important factor of vehicle energy consumption. Meanwhile, as the mechanical transmission system is highly nonlinear, and the calculation of individual components is difficult, we focus on the input and output of the entire mechanical system, instead. The input power is from the traction motors, which is calculated by Eq. (15), and the output power is calculated from the horizontal vehicle movement, which is derived by Eq. (16). T_{ipm}, T_{im} are electromagnetic torque generated by IPM and IM; $\omega_{ipm}, \omega_{im}$ are the rotational speed of IPM and IM; F_trac is the estimated total traction force; and v is the vehicle speed.

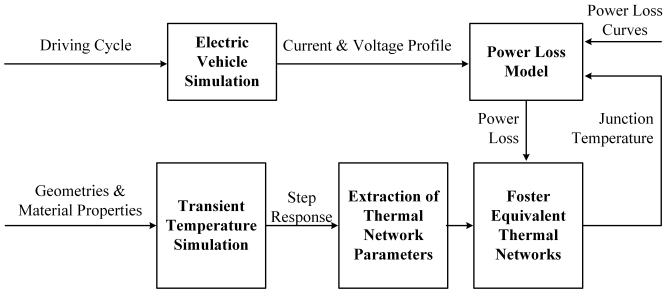

Fig. 7: Instant power loss calculation procedures using electro-thermal model.

$$p_{in} = T_{ipm} \cdot \omega_{ipm} + T_{im} \cdot \omega_{im} \quad \text{(input power)} \quad (15)$$

$$p_{out} = F_{trac} \cdot v \quad \text{(output power)} \quad (16)$$

D. Battery Loss

The battery resistance model is adopted to calculate the energy and power information during charging and discharging. The energy relationship is derived from Eq. (17) and Eq. (18),where p_s, p_1 are the battery input power and output power; U_s, I are the battery voltage and current; and R is the internal resistance.

$$p_s = U_s \cdot I = p_1 + I^2 \cdot R \quad \text{(power equation)} \quad (17)$$

$$I = \frac{U_s - \sqrt{U_s^2 - 4p_1R}}{2R} \quad \text{(current solution)} \quad (18)$$

With the power information, the Sate of Charge (SOC) could be calculated by Eq. (19)

$$SOC = \frac{\int_0^t p_s dt}{C_s} \quad (19)$$

where C_s is the total capacity of the battery.

VI. Simulation Results

The simulation testbed is realised through OPAL-RT OP5700 real-time simulator shown in Fig. 8 and validated by the New European Driving Cycle (NEDC). The simulation results will be discussed in detailed from the following aspects: mechanical performance, electrical performance, energy monitor, and attack case study.

A. Mechanical Performance

Fig. 9 shows the profiles of vehicle speed, front wheel torque, and front wheel slip under NEDC. As shown in Fig. 9, the entire system is operating stably, the slip is within 0.01, which is conform to the reality with a good road condition.

B. Electrical Performance

Fig. 10 shows the profiles of IPM three phase current, IPM torque, and IPM traction inverter loss under piece-wise NEDC. As shown in Fig. 10, the torque ripple is less than 5%. The total harmonic distortion of the three phase current is not calculated

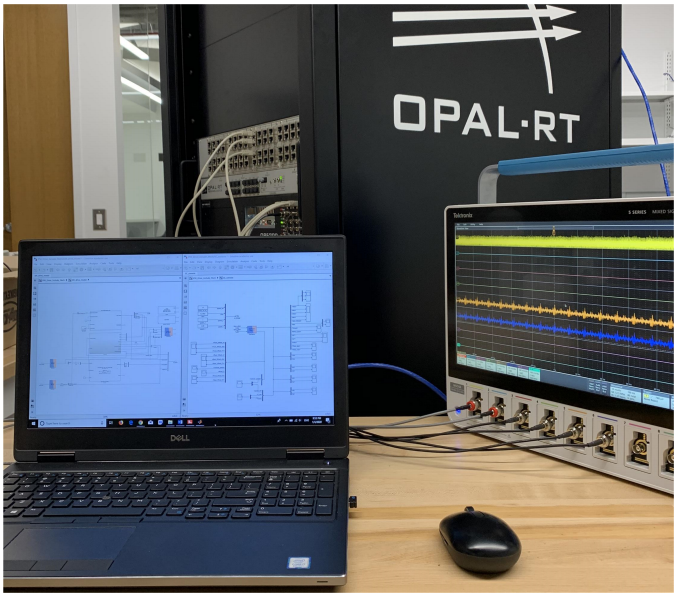

Fig. 8: OPAL-RT HIL real-time simulation testbed

due to the fact that the fundamental frequency is varying with respect to the vehicle speed. Nevertheless, the current distortion is minor from Fig. 10. Meanwhile, it could also be seen that the power loss of traction inverter is fluctuating around certain values.

C. Energy Monitor

Fig. 11 shows the profiles of vehicle speed, total efficiency, and subsystem efficiency under piece-wise NEDC. It could be seen that the traction inverter is operating with the efficiency over 95% and both traction motors are operating with the efficiency around 90%. In addition, the total traction motor drive's efficiency is around 87%, which conform to the real world data.

D. Attack Case Study

Fig. 12 shows the profiles of IPM three phase current, IPM d-axis current, and IPM q-axis current when the IPM drive is under a malicious attack. In this case, the attack happens at 108.00s, which disables the current controller of IPM by injecting false values into the phase A current sensor feedback signals. As shown in Fig. 12, when the attack happens, the three phase current will be seriously distorted and the d- and q- axis current will also be deviated from their normal values.

According to the simulation results, the strength of this platform could be summarized as follows:

1) Features from multiple physical domains of the electric vehicle powertrain could be reflected;
2) Energy consumption information could be calculated for further analysis;
3) Real-time simulation could realize the simulation of long-period driving cycles;
4) Physics-based features and patterns could be generated for cyber attack scenarios.

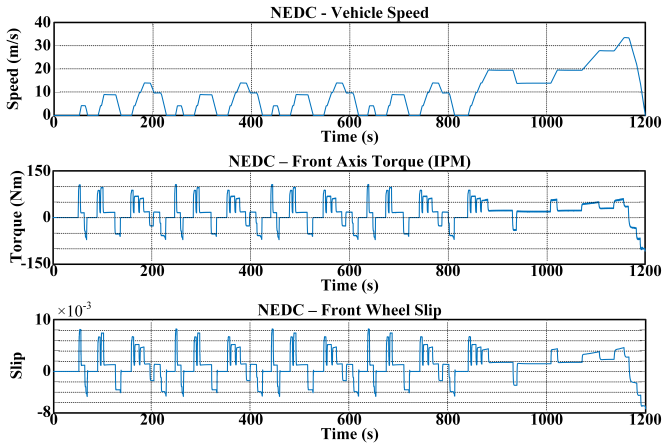

Fig. 9: Simulation results: profiles of vehicle speed, front wheel torque, and front wheel slip under NEDC.

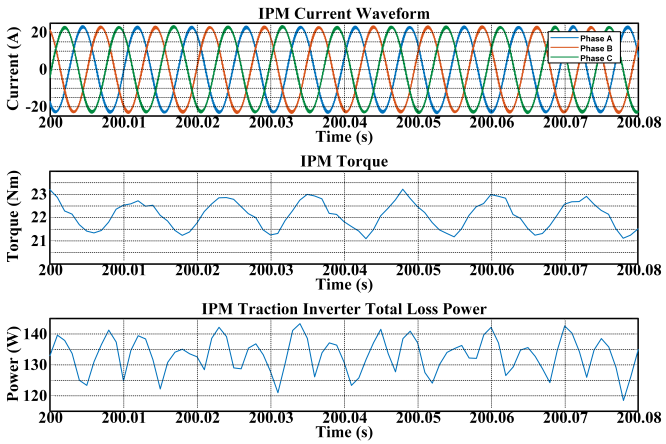

Fig. 10: Simulation results: profiles of IPM three phase current, IPM torque, and IPM traction inverter loss under piece-wise NEDC.

VII. Summary and Conclusions

In this paper, we proposed a hardware-in-the-loop real-time simulation testbed for electric vehicle powertrain. It consists of multiple physical domains and critical details. The significance of this HIL testbed is summarized as follows:

1) This testbed could provide a simple and effective method to validate the research of security and reliability issues in the electric vehicle powertrain;
2) The modularization of this testbed makes it easy to adapt different types of electric vehicle powertrain and makes it possible to conduct hardware-in-the-loop simulation for each subsystem;
3) The data collected from the real-time simulation could be a valuable resource for the data-driven research related to the performance, reliability, security and resilience in electric vehicle powertrains.

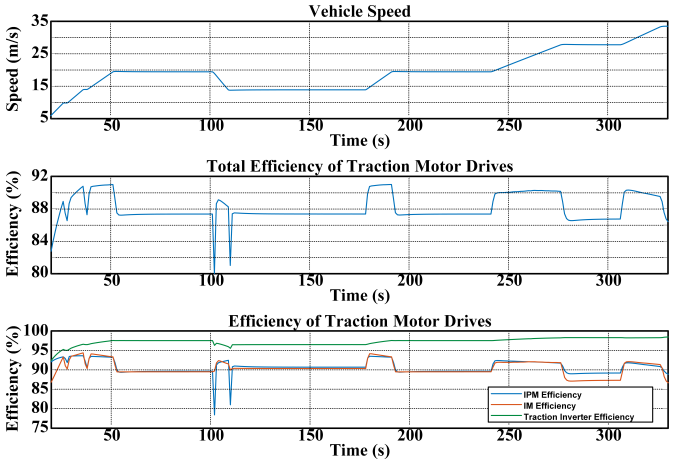

Fig. 11: Simulation results: profiles of vehicle speed, total efficiency, and subsystem efficiency under piece-wise NEDC.

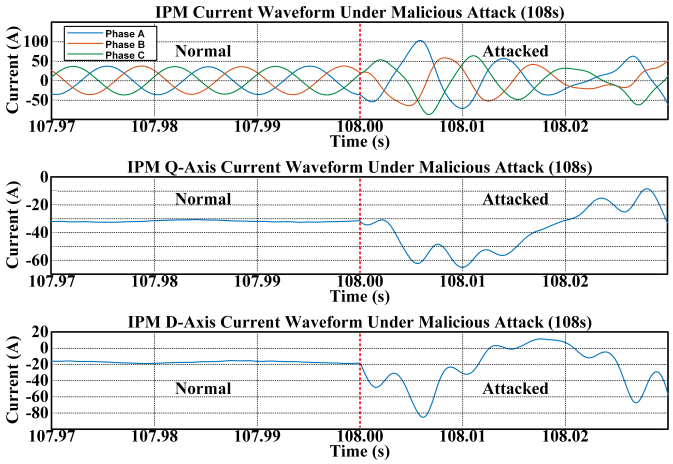

Fig. 12: Simulation results: profiles of IPM three phase current, IPM d-axis current, and IPM q-axis current when the IPM drive is under malicious attack.

ACKNOWLEDGMENT

Our research is sponsored by NSF-ECCS-1946057.

REFERENCES

[1] K. Koscher, A. Czeskis, F. Roesner, S. Patel, T. Kohno, S. Checkoway, D. McCoy, B. Kantor, D. Anderson, H. Shacham *et al.*, "Experimental security analysis of a modern automobile," in *2010 IEEE Symposium on Security and Privacy*. IEEE, 2010, pp. 447–462.

[2] B. Yang, L. Guo, F. Li, J. Ye, and W. Song, "Impact analysis of data integrity attacks on power electronics and electric drives," IEEE Transportation Electrification Conference and Expo (ITEC), Detroit, MI, 2019.

[3] ——, "Vulnerability assessments of electric drive systems due to sensor data integrity attacks," *IEEE Transactions on Industrial Informatics*, 2019.

[4] O. Vuković and G. Dán, "Detection and localization of targeted attacks on fully distributed power system state estimation," in *2013 IEEE International Conference on Smart Grid Communications (SmartGridComm)*. IEEE, 2013, pp. 390–395.

[5] S. Cui, Z. Han, S. Kar, T. T. Kim, H. V. Poor, and A. Tajer, "Coordinated data-injection attack and detection in the smart grid: A detailed look at enriching detection solutions," *IEEE Signal Processing Magazine*, vol. 29, no. 5, pp. 106–115, 2012.

[6] C. Kwon, W. Liu, and I. Hwang, "Security analysis for cyber-physical systems against stealthy deception attacks," in *2013 American control conference*. IEEE, 2013, pp. 3344–3349.

[7] G. Dan and H. Sandberg, "Stealth attacks and protection schemes for state estimators in power systems," in *2010 first IEEE international conference on smart grid communications*. IEEE, 2010, pp. 214–219.

[8] A. Broggi, P. Cerri, M. Felisa, M. C. Laghi, L. Mazzei, and P. P. Porta, "The vislab intercontinental autonomous challenge: an extensive test for a platoon of intelligent vehicles," *International Journal of Vehicle Autonomous Systems*, vol. 10, no. 3, pp. 147–164, 2012.

[9] D. Wu, D. I. Arkhipov, M. Kim, C. L. Talcott, A. C. Regan, J. A. McCann, and N. Venkatasubramanian, "Addsen: Adaptive data processing and dissemination for drone swarms in urban sensing," *IEEE transactions on computers*, vol. 66, no. 2, pp. 183–198, 2016.

[10] S. Martini, D. Di Baccio, F. A. Romero, A. V. Jiménez, L. Pallottino, G. Dini, and A. Ollero, "Distributed motion misbehavior detection in teams of heterogeneous aerial robots," *Robotics and Autonomous Systems*, vol. 74, pp. 30–39, 2015.

[11] R. Mitchell and R. Chen, "Adaptive intrusion detection of malicious unmanned air vehicles using behavior rule specifications," *IEEE Transactions on Systems, Man, and Cybernetics: Systems*, vol. 44, no. 5, pp. 593–604, 2013.

[12] B. Tabbache, Y. Aboub, K. Marouani, A. Kheloui, and M. E. H. Benbouzid, "A simple and effective hardware-in-the-loop simulation platform for urban electric vehicles," in *2012 First International Conference on Renewable Energies and Vehicular Technology*, March 2012, pp. 251–255.

[13] W. Hongyu, Y. Zhiqiang, F. Yong, Q. Yunqian, and L. Zhiming, "Development of pure electric vehicle powertrain controller based on hardware in the loop platform," in *2015 6th IEEE International Conference on Software Engineering and Service Science (ICSESS)*, 2015, pp. 498–502.

[14] J. F. B. Araújo, H. M. Pedrosa, M. C. B. P. Rodrigues, and P. G. Barbosa, "Real-time hardware-in-the-loop simulation of components of an electric vehicle powertrain: Modeling and implementation," in *2016 12th IEEE International Conference on Industry Applications (INDUSCON)*, Nov 2016, pp. 1–7.

[15] M. Awadallah, P. Tawadros, P. Walker, and N. Zhang, "Hardware-in-the-loop simulation for the design and testing of motor in advanced powertrain applications," in *2018 IEEE 27th International Symposium on Industrial Electronics (ISIE)*, June 2018, pp. 817–824.

[16] J. Ye, K. Yang, H. Ye, and A. Emadi, "A fast electro-thermal model of traction inverters for electrified vehicles," *IEEE Transactions on Power Electronics*, vol. 32, no. 5, pp. 3920–3934, May 2017.

[17] H. Ye, K. Yang, H. Ge, P. Magne, and A. Emadi, "A drive cycle based electro-thermal analysis of traction inverters," in *2014 IEEE Transportation Electrification Conference and Expo (ITEC)*, June 2014, pp. 1–6.